Received: 30 August 2021 | Revised: 1 December 2021 | Accepted: 23 December 2021

DOI: 10.1111/mpp.13184

Molecular Plant Pathology WILEY

ORIGINAL ARTICLE

Suppression of XopQ–XopX-induced immune responses of rice by the type III effector XopG

Sohini Deb[1,2] | C. G. Gokulan[1] | Rajkanwar Nathawat[1] | Hitendra K. Patel[1] | Ramesh V. Sonti[1,3]

[1]CSIR - Centre for Cellular and Molecular Biology (CSIR-CCMB), Hyderabad, India

[2]Department of Plant and Environmental Sciences, University of Copenhagen, Frederiksberg C, Denmark

[3]Indian Institute of Science Education and Research (IISER) Tirupati, Tirupati, India

Correspondence
Ramesh V. Sonti, CSIR - Centre for Cellular and Molecular Biology (CSIR-CCMB), Hyderabad 500007, India.
Email: sonti@ccmb.res.in

Funding information
Council of Scientific and Industrial Research, India, Grant/Award Number: MLP0121; Science and Engineering Research Board, Grant/Award Number: GAP0444

Abstract

Effectors that suppress effector-triggered immunity (ETI) are an essential part of the arms race in the co-evolution of bacterial pathogens and their host plants. *Xanthomonas oryzae* pv. *oryzae* uses multiple type III secretion system (T3SS) secreted effectors such as XopU, XopV, XopP, XopG, and AvrBs2 to suppress rice immune responses that are induced by the interaction of two other effectors, XopQ and XopX. Here we show that each of these five suppressors can interact individually with both XopQ and XopX. One of the suppressors, XopG, is a predicted metallopeptidase that appears to have been introduced into *X. oryzae* pv. *oryzae* by horizontal gene transfer. XopQ and XopX interact with each other in the nucleus while interaction with XopG sequesters them in the cytoplasm. The XopG E76A and XopG E85A mutants are defective in interaction with XopQ and XopX, and are also defective in suppression of XopQ–XopX-mediated immune responses. Both mutations individually affect the virulence-promoting ability of XopG. These results indicate that XopG is important for *X. oryzae* pv. *oryzae* virulence and provide insights into the mechanisms by which this protein suppresses ETI in rice.

KEYWORDS
effector, effector-triggered immunity, resistance, rice, *Xanthomonas oryzae* pv. *oryzae*, XopG, XopQ, XopX

1 | INTRODUCTION

The arms race between hosts and pathogens drives the co-evolution of both interacting partners. Upon infection by microbial pathogens, a first layer of the plant defence response is triggered by recognition either of specific features associated with microbe-associated molecular patterns or of damage-associated molecular patterns that are released from the plant cell itself (Jones & Dangl, 2006). Gram-negative plant-pathogenic bacteria employ their type III secretion system (T3SS) to translocate a set of effector proteins into the infected host cell, which act to suppress the first layer of the plant immune system. In turn, plants have developed a second layer of the immune system in which resistance genes interact with microbial effector proteins and activate effector-triggered immunity (ETI) responses (Ma et al., 2006; Rohmer et al., 2004). Pathogens may counter this by modifying or losing the effector protein or acquiring new effectors that suppress this ETI to avoid detection. For example, a subset of effectors has been identified that suppress immunity induced by the HopZ3 effector of *Pseudomonas* (Rufián et al., 2018).

The *Pseudomonas* effector HopD1 has also been shown to have a role in the suppression of ETI (Block et al., 2014).

The role of horizontal gene transfer in effector acquisition has been well studied, wherein multiple type III effector genes are located in pathogenicity islands or are associated with mobile elements (Kim et al., 1998). This leads to the evolution of the type III effector repertoire of pathogens, which is central to the co-evolutionary arms race.

Xanthomonas oryzae pv. *oryzae* is a vascular pathogen of rice and has a T3SS, secreting around 24 non-TAL type III effectors during its pathogenesis. These injected effectors target different host-cell processes to allow efficient host colonization. Four of its type III effectors, namely Xanthomonas outer protein Q (XopQ), XopN, XopX, and XopZ, have been shown to suppress immune responses in rice induced by the action of cell wall-degrading enzymes (Sinha et al., 2013). However, coexpression of two of these effectors, XopQ and XopX, was shown to induce rice immune responses (Deb et al., 2020). Furthermore, a subset of five *X. oryzae* pv. *oryzae* type III effectors, namely XopU, XopV, XopP, XopG, and AvrBs2, was found to suppress XopQ–XopX-induced immune responses (Deb et al., 2020).

Out of the effectors that suppress XopQ–XopX-induced immune responses, AvrBs2 and XopV were observed to be a part of the core effectors in multiple strains of *X. oryzae* (Midha et al., 2017). XopV, XopU, and XopP have also been shown to be ubiquitously present in *X. oryzae* pv. *oryzae* and *X. oryzae* pv. *oryzicola* strains (Hajri et al., 2009). However, the XopG effector protein, a predicted zinc-dependent metallopeptidase, is variably present in multiple strains of *Xanthomonas* (Midha et al., 2017), which may also be indicative of its introduction through a horizontal gene transfer event.

Homologs of XopG in the enteropathogenic *Escherichia coli*, NleC and NleD, are Zn-endopeptidases that target the NF-κB and c-Jun N-terminal kinase (JNK) pathways, respectively (Baruch et al., 2011). The HopH1 (a homolog of *X. oryzae* pv. *oryzae* XopG) effector of the plant pathogen *Pseudomonas syringae* also shows significant but lower sequence similarity to NleD (Baruch et al., 2011). HopH1 may contribute to virulence on host plants, as deletion of *hopH1* along with the effector *hopC1* from this pathogen reduces lesion formation and growth in *Arabidopsis* and tomato (Wei et al., 2007).

In this work we show that XopU, XopV, XopP, XopG, and AvrBs2 interact with both XopQ and XopX. The XopG effector appears to have been introduced into *X. oryzae* pv. *oryzae* by horizontal gene transfer. XopQ and XopX interact with each other in the nucleus while interaction with XopG sequesters them in the cytoplasm. The XopG E76A and XopG E85A mutants are defective in interaction with XopQ and XopX and are also defective in suppression of XopQ–XopX-mediated immune responses. Both mutations individually affect the virulence-promoting ability of XopG. These results indicate that XopG is important for *X. oryzae* pv. *oryzae* virulence and provide insights into the mechanisms by which the protein suppresses XopQ–XopX-induced ETI in rice.

2 | RESULTS

2.1 | Expression of *xopU*, *xopV*, *xopP*, *xopG*, *avrBs2*, *xopQ*, and *xopX* of *X. oryzae* pv. *oryzae* at different time points during infection

In a previous study, the XopU, XopV, XopP, XopG, and AvrBs2 proteins were found to suppress XopQ–XopX-mediated immune responses in rice (Deb et al., 2020). We have now examined the expression of *xopQ*, *xopX*, and the suppressors *xopU*, *xopV*, *xopP*, *xopG*, and *avrBs2* in planta after infection with the wild-type *X. oryzae* pv. *oryzae* strain BXO43. *xopQ* was expressed up to 6 days postinfection (dpi) (Figure 1b), a period in which expression of *xopX* was also high (Figure 1a). Coexpression of these two effectors is consistent with the possibility of physical interaction between the two proteins. Interestingly, the pattern of expression of four of the five suppressor effectors, *xopU*, *xopV*, *xopP*, and *avrBs2*, was also observed to overlap with *xopQ*/*xopX* expression, wherein increased expression of these effector protein genes could be detected in the initial stages of infection (Figure 1a,b). As also observed for *xopQ* and *xopX*, the expression of these effectors was seen to reduce at 6 dpi. However, *xopG* expression increased between 2 and 6 dpi (Figure 1b).

2.2 | XopU, XopV, XopP, XopG, and AvrBs2 interact physically with XopQ and XopX

We assessed the ability of the XopU, XopV, XopP, XopG, and AvrBs2 proteins to interact with XopQ and XopX. *xopQ* and *xopX* were cloned with the binding domain in a yeast two-hybrid vector, yielding BD::XopQ and BD::XopX. *xopU*, *xopV*, *xopP*, *xopG*, and *avrBs2* were cloned with the activation domain, yielding AD::XopU, AD::XopV, AD::XopP, AD::XopG, and AD::AvrBs2, respectively. A pairwise yeast two-hybrid analysis indicated that all the five effectors interacted individually with both XopQ (Figure 2a) and XopX (Figure 2b).

In order to confirm this, we performed a bimolecular fluorescence complementation (BiFC) assay. For this, *xopQ* and *xopX* were cloned in the BiFC vector containing the N-terminal region of the Venus fluorescent protein (nVFP), while *xopU*, *xopV*, *xopP*, *xopG*, and *avrBs2* were cloned in the BiFC vector containing the C-terminal region of VFP (cVFP). Coinfiltration of nVFP::XopQ or nVFP::XopX with cVFP fusions of these five suppressors indicated that, individually, they interacted in planta with XopQ (Figure 2c) and XopX (Figure 2d).

To further confirm these interactions in planta, we performed an affinity pulldown experiment. *Agrobacterium tumefaciens* AGL1 harbouring either pMDC7::*xopQ*-6×His or pMDC7::*xopX*-6×His along with either pH7WGF2::*gus* (EGFP::*gus*) or EGFP fused with the effectors XopU, XopV, XopP, XopG, or AvrBs2 was cocultured with rice roots. Immunoblotting of the eluted soluble proteins bound to Ni^{2+}-nitrilotriacetic acid (NTA) superflow agarose slurry using anti-His or anti-GFP antibody revealed that EGFP::XopU, EGFP::XopV, and EGFP::XopG, but not EGFP::GUS, were pulled down by XopQ-His

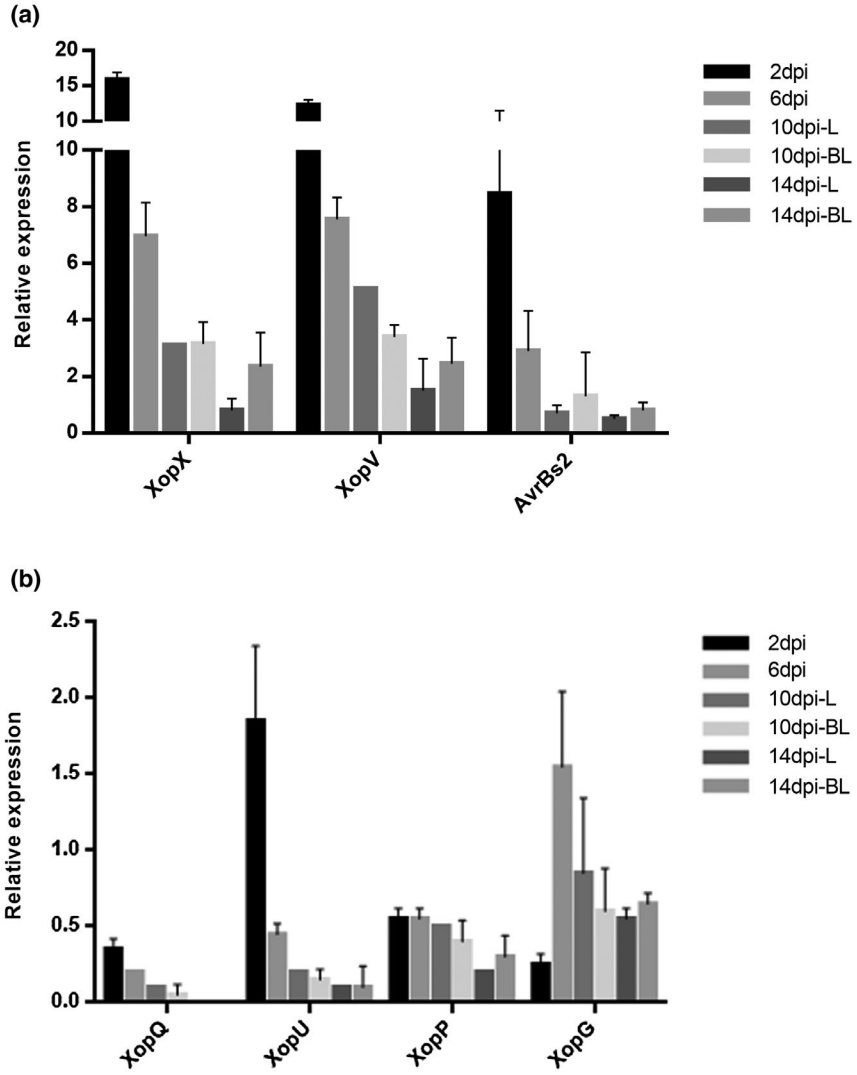

FIGURE 1 The *xopU*, *xopV*, *xopP*, *xopG*, and *avrBs2* genes coexpressed with *xopQ* and *xopX*. Expression analysis of effector protein genes in planta after *Xanthomonas oryzae* pv. *oryzae* BXO43 infection. Relative expression levels of (a) *xopX*, *xopV*, and *avrBs2* and (b) *xopQ*, *xopU*, *xopP* and *xopG* were calculated after clip inoculation of TN1 rice leaves with BXO43 at different time points: 2 days postinfection (dpi), 6 dpi, 10 dpi L (in the lesion), 10 dpi BL (in the leading edge of infection; below lesion), 14 dpi L, or 14 dpi BL. Each bar represents the average relative expression level, and the error bars indicate standard deviation. 16S rRNA was used as internal control. Relative expression levels were calculated by using the $2^{-\Delta Ct}$ method

and XopX-His (Figure 2e–g). This further indicates that XopU, XopV, and XopG interact with XopQ and XopX in planta. Interaction of XopP and AvrBs2 could not be confirmed by pulldown, possibly due to low levels of expression of these proteins in rice.

2.3 | XopG is a predicted metallopeptidase that may have been introduced into *X. oryzae* pv. *oryzae* by an event of horizontal gene transfer

The XopG effector is a predicted metallopeptidase, having the conserved domain HEXXH (HELIH; spanning residues 84–88). It has homologs in multiple plant pathogens, including *Pseudomonas* and *Ralstonia* (Figure 3a). In *Xanthomonas*, XopG is present in the Asian *X. oryzae* pv. *oryzae* L-IV strains (except IXO97), Asian *X. oryzae* pv. *oryzae* L-II strains, and Asian *X. oryzae* pv. *oryzae* L-I strains (except IXO134). It is absent in the US *X. oryzae*, African *X. oryzae* pv. *oryzae* and *X. oryzae* pv. *oryzicola*, and Asian *X. oryzae* pv. *oryzae* L-V strains and is absent or has partial sequences/contig break/disruption or frameshift mutations in Asian *X. oryzae* pv. *oryzae* L-III strains (Midha et al., 2017). The presence of this effector gene in diverse plant-pathogenic bacteria and in some, but not all, *Xanthomonas* indicates the possibility that this gene may have been introduced into *X. oryzae* pv. *oryzae* by an event of horizontal gene transfer. The *xopG* locus is flanked by multiple transposase genes, which is indicative of a hotspot of horizontal gene transfer (Figure 3b). Interestingly, *xopG* has a G + C content of 52%, which is significantly lower than the *X. oryzae* pv. *oryzae* average G + C content of 63.7% (Kaur et al., 2019) (Figure 3b). This further suggests that *xopG* might have been acquired by horizontal gene transfer. We also examined the codon usage pattern of the *xopG* gene and observed that the codon usage pattern of *xopG* was significantly different from that of the housekeeping genes of *X. oryzae* pv. *oryzae* (Figure 3c). It appeared closer to that of the lipopolysaccharide (LPS) cluster of *X. oryzae* pv. *oryzae*, which has been earlier shown to have the signature features of a genomic island (Patil & Sonti, 2004).

2.4 | XopG sequesters both XopQ and XopX in the cytoplasm

We next assessed the localization of the XopQ–XopG and XopX–XopG complexes after interaction. Subcellular localization prediction

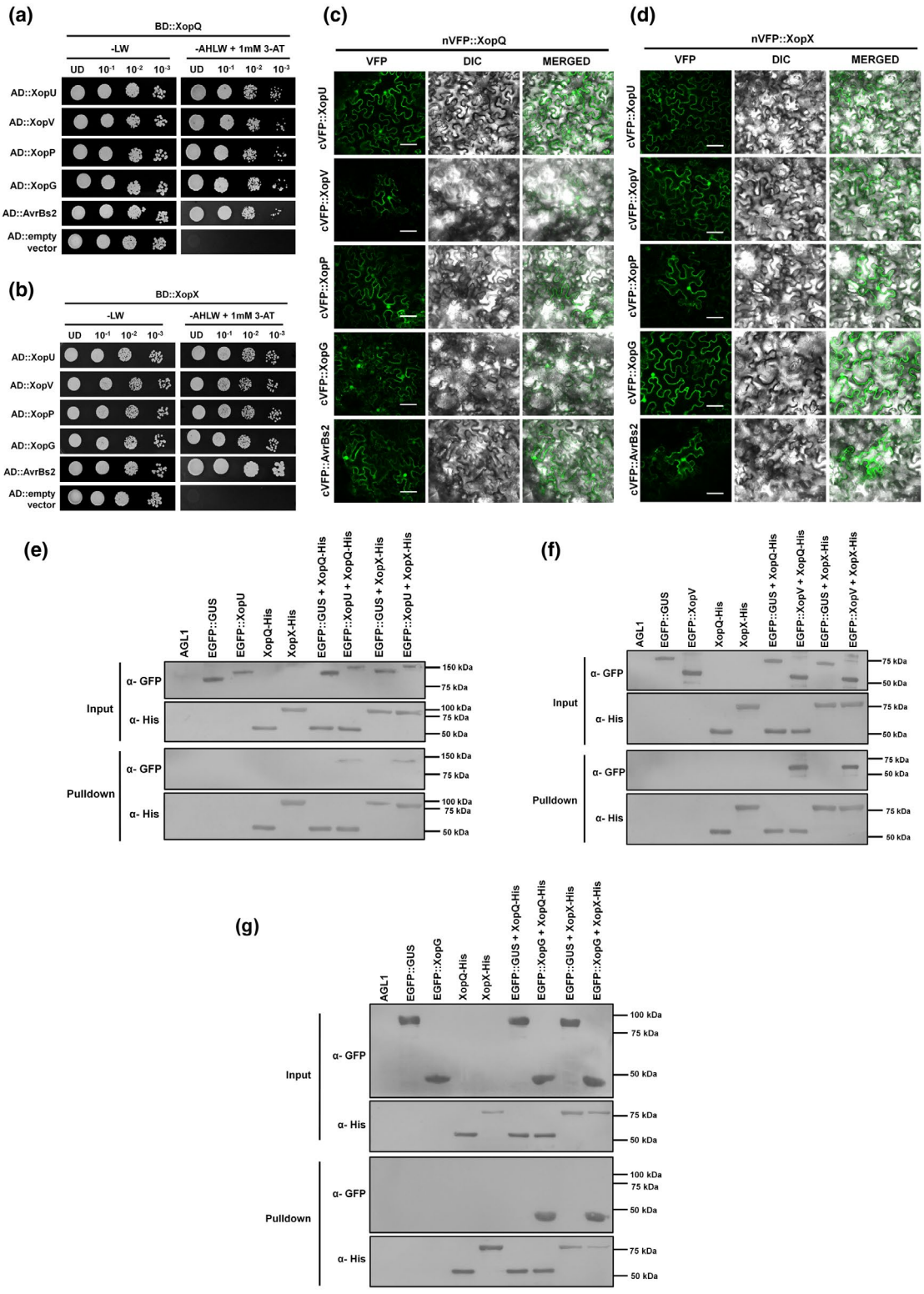

FIGURE 2 Legend on next page

by NLS Mapper software (Kosugi et al., 2009) indicated that XopG contains a C-terminal nuclear localization signal and may be nucleo-cytoplasmic (Figure S1a). This was confirmed by a localization study of the EGFP-tagged XopG protein in onion epidermal cells, wherein XopG was found to be mainly localized to the cytoplasm but was also observed in the nucleus (Figure S1b). The XopQ–XopX interaction was earlier shown to take place in the nucleus (Deb et al., 2020). Interestingly, the interaction of XopG with either XopQ or XopX seemed to take place exclusively in the cytoplasm (Figure 4). This may indicate that XopG sequesters the XopQ and XopX proteins in the cytoplasm, thus preventing their colocalization and interaction in the nucleus.

FIGURE 2 The suppressors of XopQ–XopX-mediated immune responses interact physically with both XopQ and XopX. (a, b) Yeast strain PJ694a containing pDEST32 vector expressing a binding domain (BD) fusion with (a) XopQ or (b) XopX was independently transformed with pDEST22 vector expressing an activation domain (AD) fusion with XopU, XopV, XopP, XopG, AvrBs2, or empty vector pDEST22. Transformed colonies were serially diluted and spotted on the nonselective −LW (−Leu −Trp) medium and selective −AHLW (−Ade −His −Leu −Trp) medium with 1 mM 3-amino-1,2,4-triazole (3-AT). Observations were noted after 3 days of incubation at 30°C. (c, d) For bimolecular fluorescence complementation analysis, leaves of *Nicotiana benthamiana* were syringe-infiltrated with a suspension of two *Agrobacterium tumefaciens* AGL1 strains containing vectors expressing nVFP::XopQ or nVFP::XopX and cVFP::XopU, cVFP::XopV, cVFP::XopP, cVFP::XopG, or cVFP::AvrBs2. Fluorescence was visualized in a confocal microscope at 20× magnification and excitation at 488 nm 48 h after infiltration. Scale bar, 50 μm. (e, f, g) Roots of 4-day-old rice seedlings were cocultured with AGL1 alone or AGL1 strains harbouring the gene constructs expressing EGFP::GUS, EGFP::XopU, EGFP::XopV, or EGFP::XopG, either singly or along with AGL1 strains expressing XopQ-His or XopX-His. The bound proteins were eluted using Ni^{2+}-NTA beads and immunoblotted with anti-GFP and anti-His antibodies. Expected protein molecular weight: EGFP::GUS, 92 kDa; EGFP::XopU, 133 kDa; EGFP::XopV, 61 kDa; EGFP::XopG, 42 kDa; XopQ-His, 50 kDa; XopX-His, 80 kDa

2.5 | Identification of amino acid residues necessary for interaction of XopG with XopQ and XopX

In order to understand the mechanism of interaction of XopG with XopQ and XopX, we performed a modelling and docking study of XopG with XopQ. Using SWISS-MODEL (Waterhouse et al., 2018) in the automated mode, a homology model for XopG was generated using the crystal structure of the light chain of *Clostridium botulinum* neurotoxin, serotype A (PDB ID: 2G7K) as a template, which showed 51% query cover and 33.7% identity with XopG at the protein level. A molecular docking analysis was performed for the XopG homology model and the crystal structure of XopQ (PDB ID: 4KL0) using Z-Dock server (Pierce et al., 2014). This predicted that XopQ T222 and XopG E76 might be involved in the interaction between XopQ and XopG (Figure 5a).

In order to validate our observations from the docking studies, we studied the interaction of the XopQ T222A mutant with XopG. For this, BD::XopQ T222A and AD::XopG were used. The yeast two-hybrid analysis indicated that XopQ T222A lost interaction with XopG (Figure 5b). We also tested the interaction of XopQ T222A with XopX as well as with XopU, XopV, XopP, and AvrBs2. Interestingly, XopQ T222A lost interaction with XopX, as well as with XopP and XopV. However, it retained interaction with XopU and AvrBs2 (Figure 5b).

We confirmed these observations in an in planta BiFC assay, wherein we used nVFP::XopQ or nVFP::XopQ T222A along with cVFP::XopX, cVFP::XopG, cVFP::XopU, cVFP::XopV, cVFP::XopP, or cVFP::AvrBs2. XopQ interacted with XopX, XopU, XopV, XopP, XopG, and AvrBs2. However, XopQ T222A lost interaction with XopX, XopG, XopP, and XopV, but retained the interaction with XopU and AvrBs2 (Figure 5c).

Because XopQ T222A did not interact with XopX, we investigated if the XopQ T222A mutant could induce immune responses along with XopX. An assay for programmed cell death (PCD) was performed by expressing XopQ::EGFP or XopQ T222A::EGFP along with XopX::EGFP. Expression of XopQ::EGFP, XopQ T222A::EGFP, or XopX::EGFP proteins alone did not lead to internalization of propidium iodide (PI) stain, indicating the absence of PCD. When XopQ::EGFP was coexpressed with XopX::EGFP, PI internalization, indicative of PCD, was observed. However, when XopQ T222A::EGFP was expressed along with XopX::EGFP, no PI internalization was observed (Figure 6a,b). This indicates that the XopQ T222A mutant is deficient in the induction of PCD when coexpressed with XopX. Similar results were obtained in a callose deposition experiment wherein XopQ T222A failed to induce callose deposition when coexpressed with XopX (Figure 6c,d).

2.6 | XopG E76A and XopG E85A proteins lose the ability to interact with XopQ and XopX and are also unable to suppress XopQ–XopX-induced immune responses

In order to further characterize the interaction of XopG with XopQ and XopX, we mutated XopG E76 to alanine by site-directed mutagenesis. XopG is predicted to be a Zn-metallopeptidase and has a conserved HEXXH motif. In order to explore the role of this motif in the interaction with XopQ and XopX, we mutated the E85 residue to alanine. *xopG E76A* and *xopG E85A* were cloned in the yeast two-hybrid vector pDEST22, creating the fusion proteins AD::XopG E76A and AD::XopG E85A, and assayed for interaction with BD::XopQ and BD::XopX. The XopG E76A and XopG E85A mutant proteins lost the ability to interact with both XopQ and XopX (Figure 7a,b). Expression levels of the XopG E76A and XopG E85A mutant proteins were comparable to those of wild-type XopG, as assayed by western blot in rice roots, indicating that these proteins are defective in the interaction but not in protein stability (Figure S2). We further confirmed this in a BiFC assay, wherein we used cVFP::XopG, cVFP::XopG E76A, or cVFP::XopG E85A, along with nVFP::XopQ or nVFP::XopX. Complementation of fluorescence of XopG–XopQ or XopG–XopX indicated interaction between the respective protein pairs. However, this complementation was lost between XopG E76A–XopQ, XopG E76A–XopX, XopG E85A–XopQ, and XopG E85A–XopX, indicating loss of interaction between the two protein pairs (Figure 7c).

In order to study the effect of the XopG E76A and XopG E85A mutations on the ability to suppress XopQ–XopX-mediated immune responses, we cloned *xopG E76A* and *xopG E85A* in the

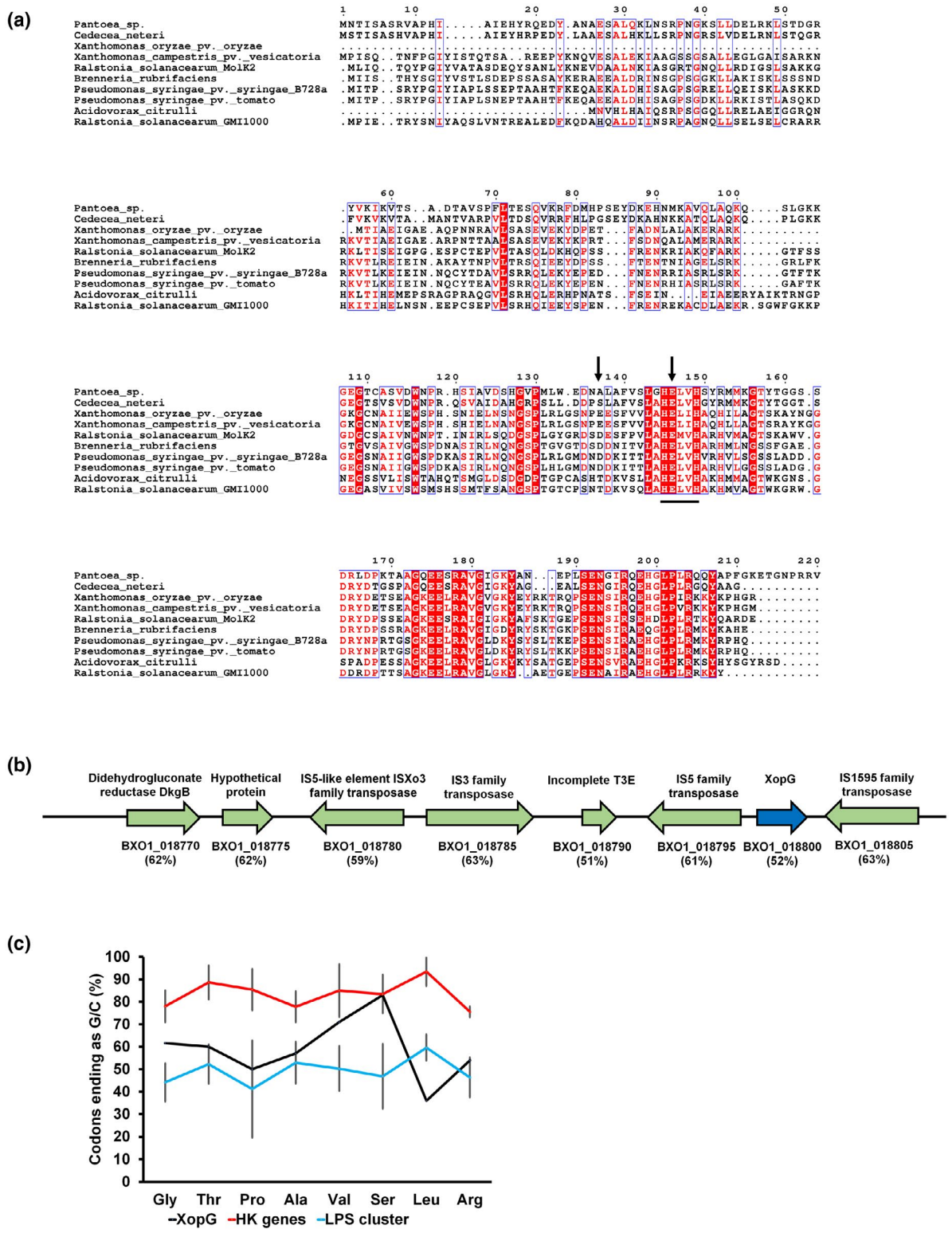

FIGURE 3 Bioinformatics analysis of XopG of *Xanthomonas oryzae* pv. *oryzae*. (a) Multiple sequence alignment of XopG using Clustal Omega. Residues marked in red denote conservation. Residues marked with a black bar indicate the conserved metallopeptidase domain. Residues marked with a black arrow indicate the E76 and E85 residues. (b) Schematic of open reading frames (ORFs) of the genomic region encompassing the *xopG* locus of *X. oryzae* pv. *oryzae* BXO1. Arrows represent the ORF and direction of transcription. The predicted ORFs upstream of the *xopG* gene encode an IS*5* family transposase, an incomplete type III effector, an IS*3* family transposase, and an IS*5*-like element IS*Xo3* family transposase. The predicted ORFs downstream of the *xopG* gene in BXO1 exhibit high similarity to an IS*1595* family transposase gene. Numbers in parentheses indicate the G + C content of the respective genes. (c) Codon usage pattern of the *xopG* gene, housekeeping (HK) genes, and the lipopolysaccharide (LPS) cluster. The error bar indicates the average codon usage pattern of the HK/LPS cluster genes

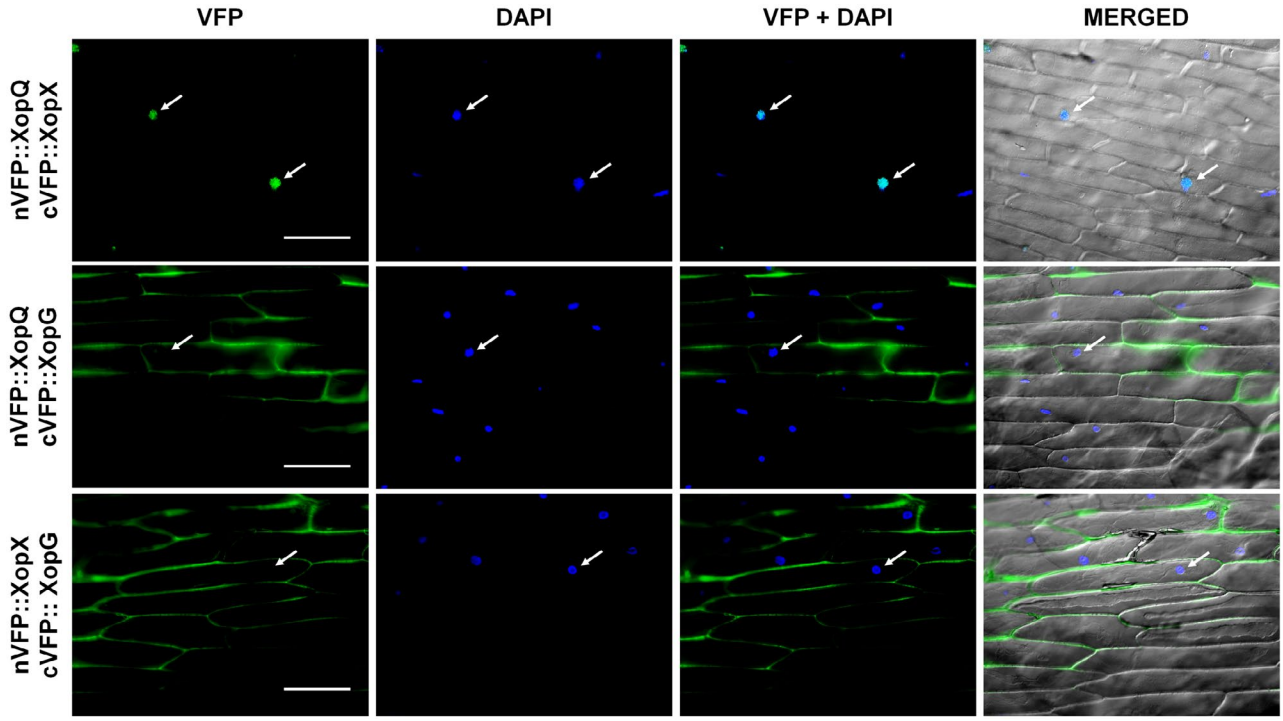

FIGURE 4 XopG sequesters XopQ and XopX in the cytoplasm. *Agrobacterium tumefaciens* AGL1 expressing one of the following was cocultured with onion epidermal peels: nVFP::XopQ + cVFP::XopX, nVFP::XopQ + cVFP::XopG, or nVFP::XopX + cVFP::XopG. Fluorescence was visualized in an epifluorescence microscope at 10× magnification and excitation at 488 nm 48 h after coculturing. Bar, 100 μm

N-terminal EGFP fusion vector pH7WGF2. As observed earlier, wild-type XopG is able to suppress XopQ–XopX-induced immune responses (Deb et al., 2020). However, both XopG E76A and XopG E85A proteins were unable to suppress XopQ–XopX-induced PCD, as reflected in the internalization of the PI stain (Figure 7d,e). Similar results were obtained in a callose deposition assay wherein XopG E76A and XopG E85A failed to suppress callose deposition induced by the coexpression of XopQ and XopX (Figure 7f,g). This suggests that interaction of XopG with XopQ and XopX may be essential for the ability of XopG to suppress XopQ–XopX-mediated immune responses.

2.7 | XopG is important for full virulence of *X. oryzae* pv. *oryzae* BXO43

In order to study the role of XopG in virulence, we clip-inoculated 60-day-old TN1 rice plants with BXO43, *xopG*$^-$, *xopG*$^-$/pHM1, *xopG*$^-$/pHM1::*xopG*, *xopG*$^-$/pHM1::*xopG E76A*, or *xopG*$^-$/pHM1::*xopG E85A*. As compared to BXO43, *xopG*$^-$ showed a significant reduction in lesion length. Addition of the empty vector pHM1 in the background of *xopG*$^-$ did not rescue the virulence deficiency of *xopG*$^-$. However, complementation with the wild-type copy of *xopG* through pHM1 restored the virulence of the *xopG*$^-$ strain. Interestingly, expression of either the *xopG E76A* or *xopG E85A* mutants through pHM1 failed to restore the virulence of the *xopG*$^-$ strain (Figure 8a,b).

3 | DISCUSSION

Plants and their pathogens participate in a co-evolutionary arms race. Plants can recognize conserved molecular features of the pathogen and induce immune responses. The type III effector repertoire of bacteria acts to block these plant immune responses (Hauck et al., 2003). In turn, resistance genes in the host may recognize these effectors and trigger defence responses. However, it is expected that there would be a strong selection pressure to avoid or suppress detection by the host. Bacterial proteins that trigger the plant defence response will be strongly selected against, and thus face the probability of being lost to avoid host recognition. This may be deleterious if the virulence factor is central for host pathogenesis. As a possible consequence, many virulence type III effectors may act to suppress the host defence response induced by other effectors. This study highlights the role of five type III effectors of *X. oryzae* pv. *oryzae*, namely XopU, XopV, XopP, XopG, and AvrBs2, in the modulation of ETI responses of rice. In the current work, we found that the expression of *xopQ* took place in the stage of establishment of the disease, up to 6 dpi. Expression of *xopX* was also seen to be high at this time, indicating that an interaction between *xopQ* and *xopX* might be possible in the early stages of disease. Coexpression of the *X. oryzae* pv. *oryzae* XopQ and XopX proteins has previously been shown to induce rice immune responses (Deb et al., 2020). In order to negate the deleterious effects of this interaction, *X. oryzae* pv. *oryzae* might employ the type III effectors XopU, XopV, XopP, XopG, and AvrBs2 to suppress XopQ–XopX-induced immune responses. Indeed,

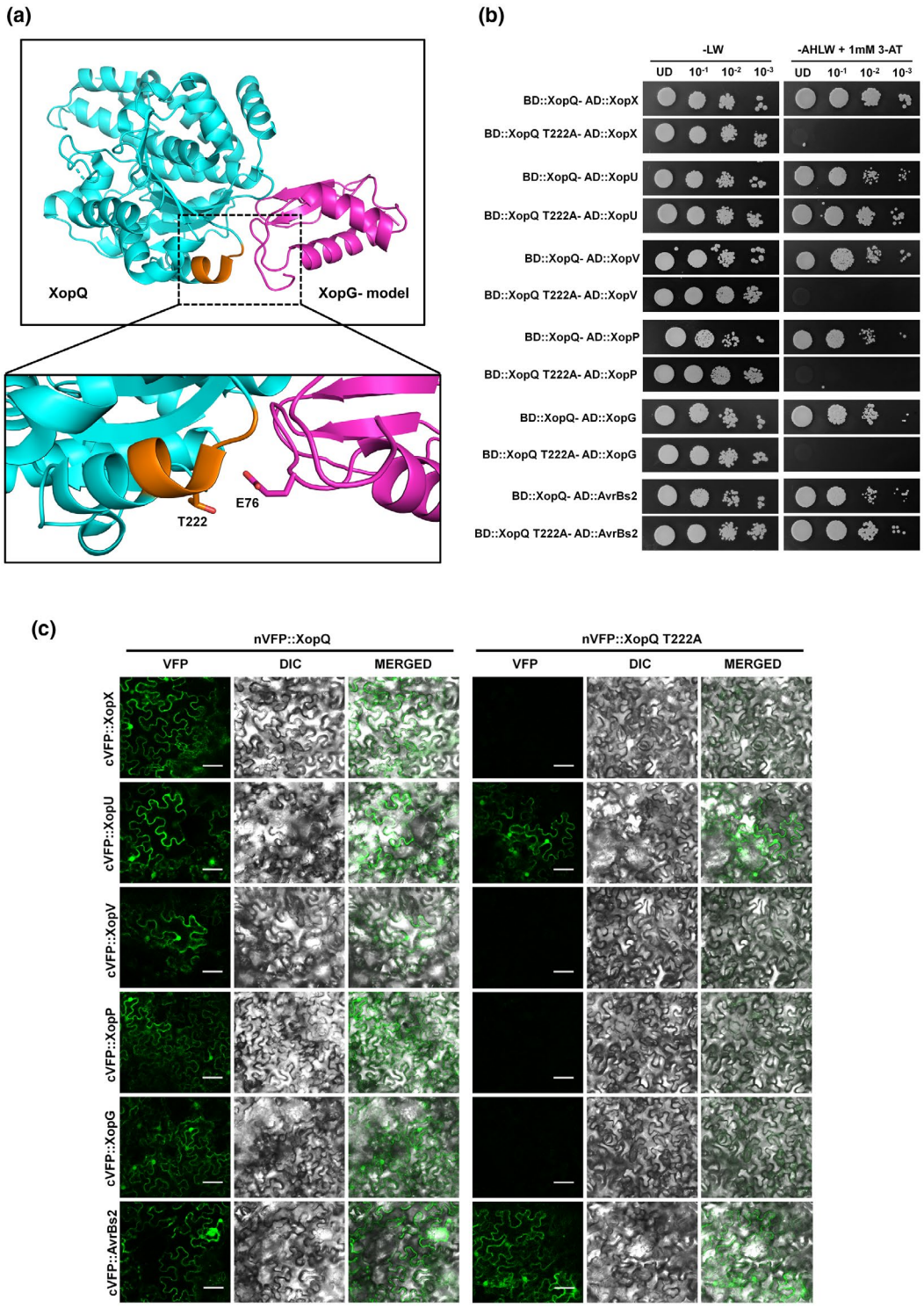

FIGURE 5 XopQ T222 is important for interaction with XopX, XopG, XopP, and XopV. (a) Docking of the XopQ crystal structure and the XopG model. The structure in blue represents the crystal structure of XopQ. The structure in pink represents the XopG model. The putative residues involved in interaction of XopQ and XopG (XopQ T222 and XopG E76) are marked in orange. (b) Yeast strain PJ694a containing pDEST32 vector expressing a binding domain (BD) fusion with XopQ or XopQ T222A was independently transformed with pDEST22 vector expressing an activation domain (AD) fusion with XopX, XopU, XopV, XopP, XopG, or AvrBs2. Transformed colonies were serially diluted and spotted on the nonselective −LW (−Leu −Trp) medium and selective −AHLW (−Ade −His −Leu −Trp) medium with 1 mM 3-amino-1,2,4-triazole (3-AT). Observations were noted after 3 days of incubation at 30°C. Similar results were obtained in three independent experiments. (c) For bimolecular fluorescence complementation analysis, leaves of *Nicotiana benthamiana* were syringe-infiltrated with a suspension of two *Agrobacterium tumefaciens* AGL1 strains containing vectors expressing nVFP::XopQ or nVFP::XopQ T222A and cVFP::XopX, cVFP::XopU, cVFP::XopV, cVFP::XopP, cVFP::XopG, or cVFP::AvrBs2. Fluorescence was visualized in a confocal microscope at 20× magnification and excitation at 488 nm 48 h after infiltration. Scale bar, 50 μm

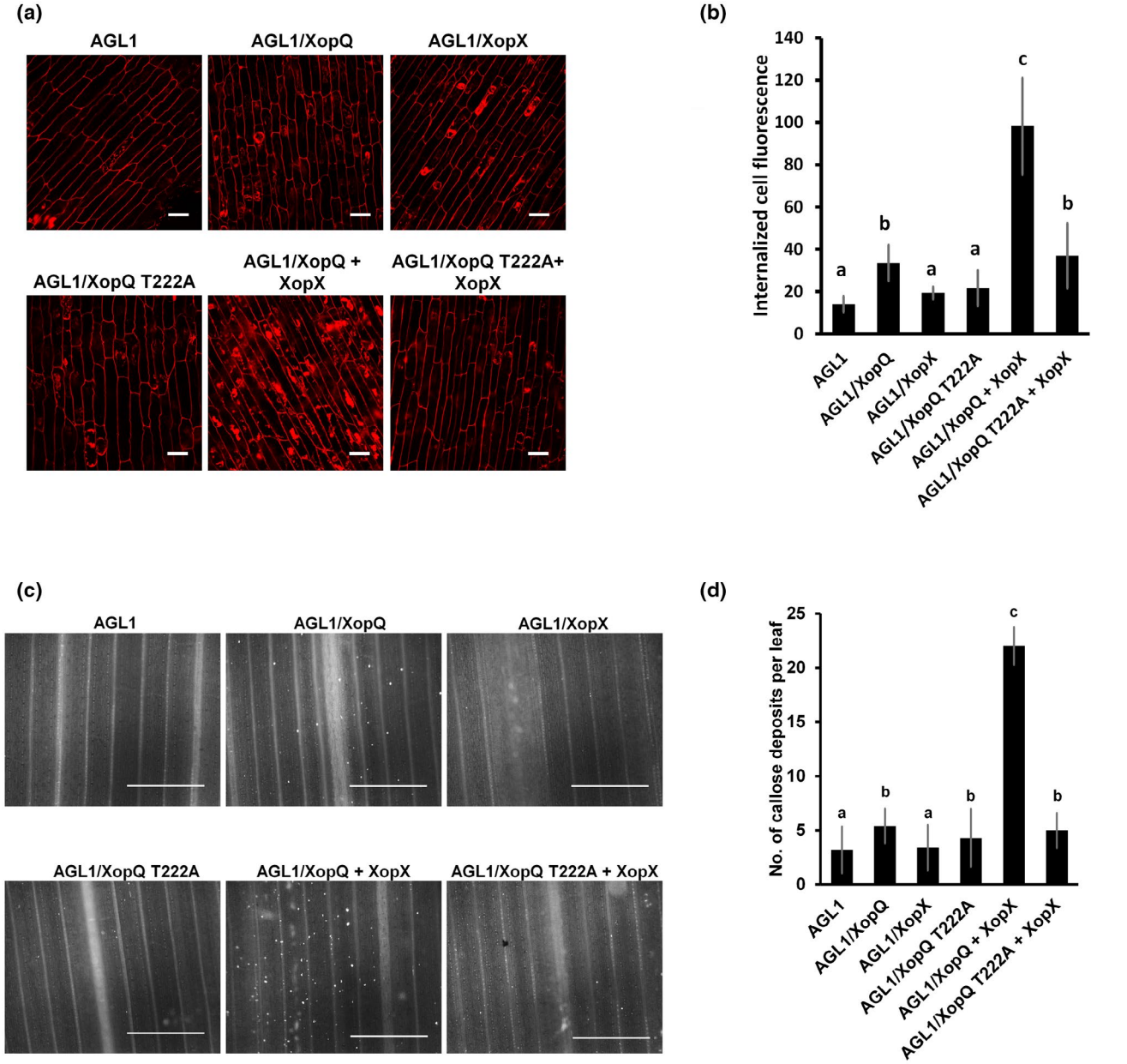

FIGURE 6 XopQ T222 is important for induction of immune responses with XopX. (a, b) Rice roots were treated with one of the following: *Agrobacterium tumefaciens* AGL1 alone or AGL1 harbouring the gene construct expressing EGFP::XopQ, EGFP::XopX, EGFP::XopQ T222A, EGFP::XopQ + EGFP::XopX, or EGFP::XopQ T222A + EGFP::XopX. Treated roots were subsequently stained with propidium iodide (PI) and observed under a confocal microscope using 63× oil immersion objectives and a He-Ne laser at 543 nm excitation to detect PI internalization. Five roots were imaged for each construct per experiment. Scale bar, 20 μm. Internalization of PI is indicative of defence response-associated programmed cell death. Internalization of PI was quantified using ImageJ. Error bars indicate the standard deviation of readings from five root cells. (c, d) For the callose deposition assay, leaves of 14-day-old rice seedlings were infiltrated with one of the following: *A. tumefaciens* AGL1 alone or AGL1 harbouring the gene construct expressing EGFP::XopQ, EGFP::XopX, EGFP::XopQ T222A, EGFP::XopQ + EGFP::XopX, or EGFP::XopQ T222A + EGFP::XopX. The leaves were stained 16 h later with aniline blue and visualized under an epifluorescence microscope (365 nm) at 10× magnification. Mean and standard deviation were calculated for the number of callose deposits observed per leaf. Error bars indicate the standard deviation of readings from five infiltrated leaves. Scale bar: 100 μm. For all graphs, columns capped with letters that are different from one another indicate that they are significantly different using the unpaired two-sided Student's *t* test ($p \leq 0.05$)

expression of four of these five suppressors, XopU, XopV, XopP, and AvrBs2, closely followed the expression pattern of XopQ and XopX, wherein increased expression was seen in the early disease stages (at 2 dpi) and gradually decreased in the later disease stages. Surprisingly, the expression of *xopG* did not conform to this pattern; a lower expression was observed at 2 dpi followed by an increase at 6 dpi. This may be a regulatory consequence of *xopQ-xopX* expression or an atypical regulation of *xopG* expression. A previous study

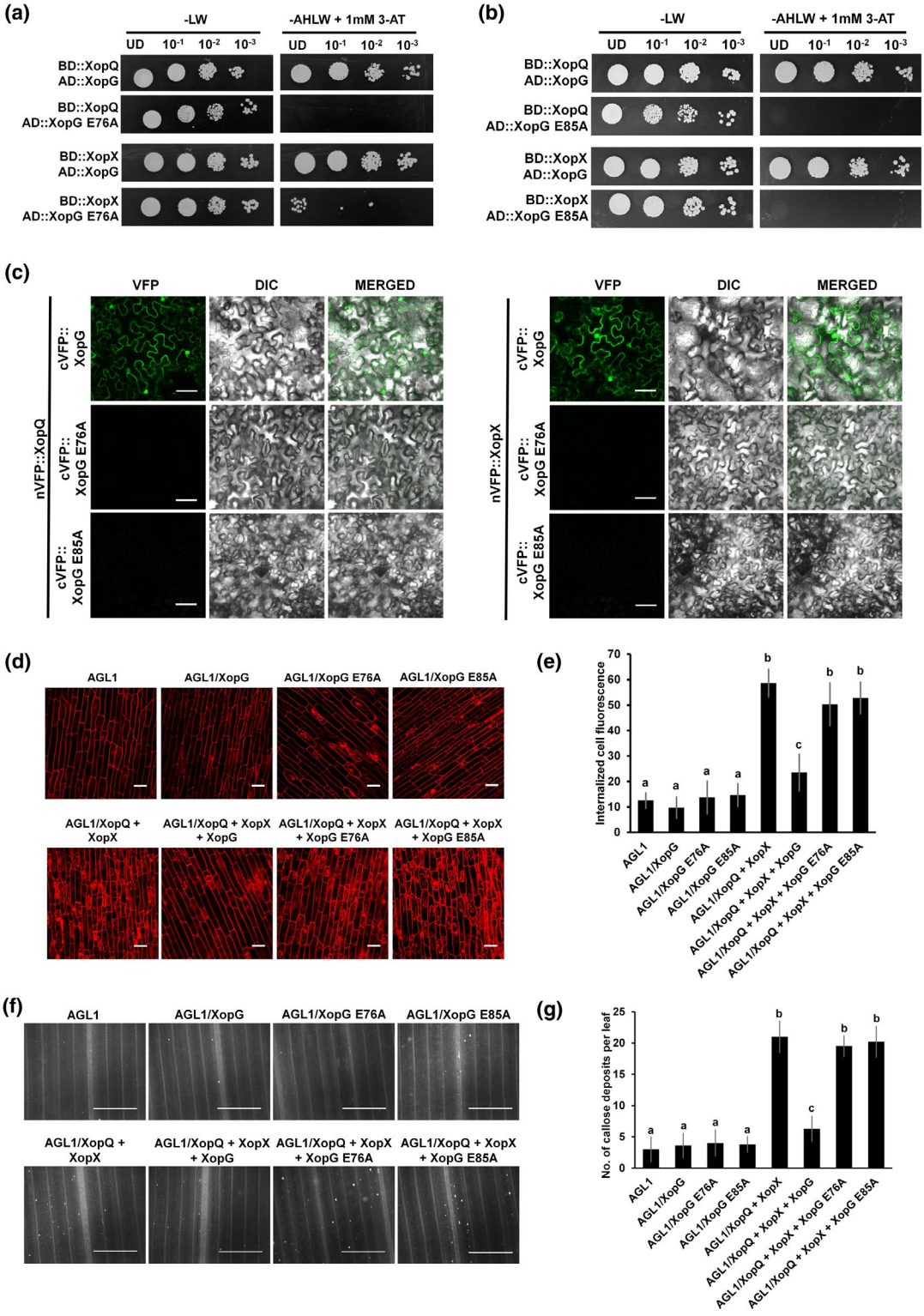

FIGURE 7 Legend on next page

has reported that the expression of *xopQ* is not regulated through the canonical *hrpG*/*hrpX* regulon (Liu et al., 2016). Expression of *xopQ* has also been observed in bacteria cultured in rich media (Deb et al., 2021).

A preliminary analysis has revealed that the promoter of *xopG* does not possess a canonical plant-inducible promoter box (PIP-box) (authors' unpublished data). Presence of the PIP-box is a characteristic feature of type III effectors whose expression is regulated by the *hrpG*/*hrpX* regulon and which are typically expressed in planta and in minimal media. Analysis of a publicly available transcriptome data set (GEO accession: GSE179029; Deb et al., 2021) also revealed that *xopG* is basally expressed in *X. oryzae* pv. *oryzae* cultured in rich media (Deb et al., 2021). This further suggests that *xopG* expression is not likely to be controlled by the *hrpG*/*hrpX* regulon.

FIGURE 7 XopG interaction with XopQ and XopX is important for suppression of XopQ–XopX-induced immune responses. (a, b) Yeast strain PJ694a containing pDEST32 vector expressing a BD fusion with XopQ or XopX was independently transformed with pDEST22 vector expressing an AD fusion with (a) XopG and XopG E76A or (b) XopG and XopG E85A. Transformed colonies were serially diluted and spotted on the nonselective −LW (−Leu −Trp) medium and selective −AHLW (−Ade −His −Leu −Trp) medium with 1 mM 3-amino-1,2,4-triazole (3-AT). Observations were noted after 3 days of incubation at 30°C. (c) For bimolecular fluorescence complementation analysis, leaves of *Nicotiana benthamiana* were syringe-infiltrated with a suspension of two *Agrobacterium tumefaciens* AGL1 strains containing vectors expressing nVFP::XopQ or nVFP::XopX and cVFP::XopG, cVFP::XopG, E76A or cVFP::XopG E85A. Fluorescence was visualized in a confocal microscope at 20× magnification and excitation at 488 nm 48 h after infiltration. Scale bar, 50 μm. (d, e) Rice roots were treated with one of the following: *A. tumefaciens* AGL1 alone or AGL1 harbouring the gene construct expressing EGFP::XopG or EGFP::XopG E76A, or pretreatment with AGL1, EGFP::XopG, EGFP::XopG E76A, or EGFP::XopG E85A, followed by treatment with EGFP::XopQ + EGFP::XopX. Treated roots were subsequently stained with propidium iodide (PI) and observed under a confocal microscope using 63× oil immersion objectives and a He-Ne laser at 543 nm excitation to detect PI internalization. Five roots were imaged for each construct per experiment. Scale bar, 20 μm. Internalization of PI is indicative of defence response-associated programmed cell death. Internalization of PI was quantified using ImageJ. Error bars indicate the standard deviation of readings from five root cells. (f, g) For the callose deposition assay, leaves of 14-day-old rice seedlings were infiltrated with one of the following: *A. tumefaciens* AGL1 alone or AGL1 harbouring the gene constructs expressing EGFP::XopG, EGFP::XopG E76A, EGFP::XopG E85A, EGFP::XopQ + EGFP::XopX, EGFP::XopQ + EGFP::XopX + EGFP::XopG, EGFP::XopQ + EGFP::XopX + EGFP::XopG E76A, or EGFP::XopQ + EGFP::XopX + EGFP::XopG E85A. The leaves were stained 16 h later with aniline blue and visualized under an epifluorescence microscope (365 nm) at 10× magnification. Mean and standard deviation were calculated for the number of callose deposits observed per leaf. Error bars indicate the standard deviation of readings from five infiltrated leaves. Scale bar: 100 μm. For all graphs, columns capped with letters that are different from one another indicate that they are significantly different using the unpaired two-sided Student's *t* test ($p \leq 0.05$)

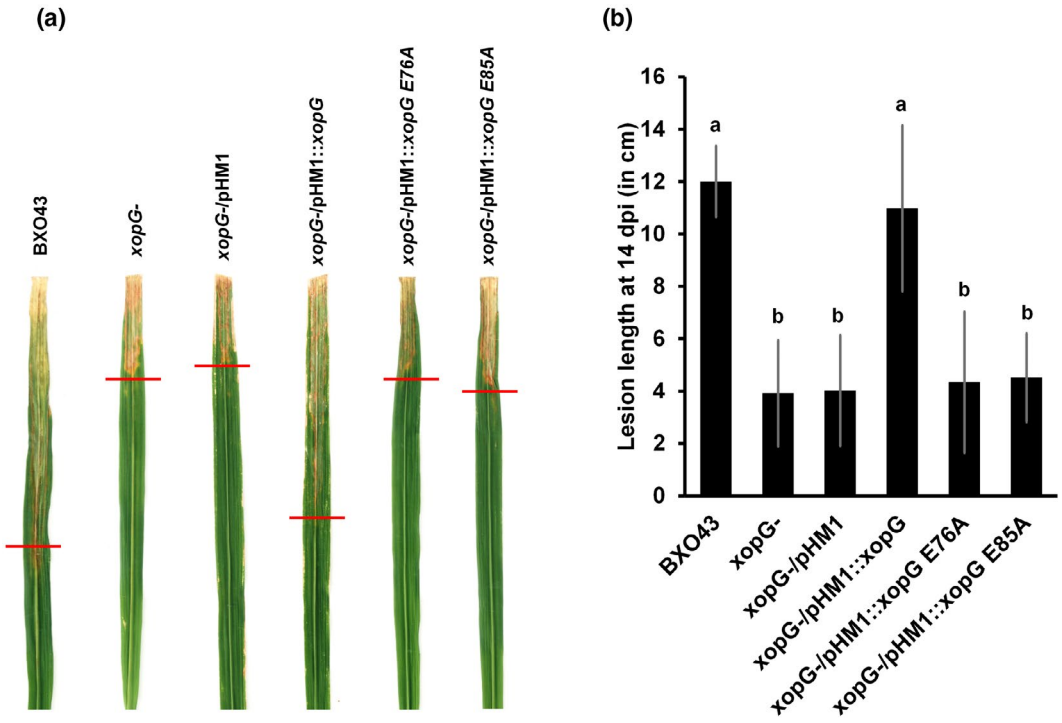

FIGURE 8 XopG interaction with XopQ and XopX is important for complete virulence of *Xanthomonas oryzae* pv. *oryzae*. (a, b) Leaves of susceptible rice TN-1 were clip-inoculated with the following strains: BXO43, *xopG*$^-$, *xopG*$^-$/pHM1, *xopG*$^-$/pHM1::*xopG*, *xopG*$^-$/pHM1::*xopG E76A*, or *xopG*$^-$/pHM1::*xopG E85A*. (a) Virulence phenotype on rice leaves. Leaves were photographed 14 days postinoculation. (b) Lesion lengths were measured at 14 dpi. Error bars indicate the standard deviation of readings from five inoculated leaves. Columns capped with letters that are different from one another indicate that they are significantly different using the unpaired two-sided Student's *t* test ($p \leq 0.05$)

Localization of the effectors during different stages of infection could determine their role in disease development. For the XopQ–XopX-induced defence responses, colocalization of the effectors is crucial. Spatial compartmentalization of XopQ and XopX during early stages of infection (e.g., 2 dpi) and a colocalization during later stages (e.g., 6 dpi) could lead to an increased expression of *xopG* at 6 dpi, in order to keep the XopQ–XopX-induced defence responses in check.

Using interaction studies, we demonstrated that XopU, XopV, XopP, XopG, and AvrBs2 interact with both XopQ and XopX, suggesting that they may have a redundant role in the suppression of

XopQ–XopX-induced immune responses. One of these five suppressors of XopQ–XopX-induced immune responses, XopG, is a predicted metallopeptidase, containing the conserved biochemical motif HEXXH. The G + C content of *xopG* is 52%, which is significantly different from the average G + C content of 64%–65% of the *Xanthomonas* genome. *xopG* also displays an altered codon usage pattern, indicative of acquisition by horizontal gene transfer. Interestingly, *xopG* is present in some, but not all, isolates of *X. oryzae*. The genomic locus encompassing *xopG* also encodes a number of transposases. All these features are consistent with the possibility that this gene may have been inherited by horizontal gene transfer.

BiFC studies indicated that interaction of XopQ–XopG and XopX–XopG occurred in the cytoplasm as opposed to the XopQ–XopX interaction that took place in the nucleus. Thus, it is possible that XopG prevents XopQ–XopX-induced immune responses by sequestering the two proteins in the cytoplasm. Molecular docking studies indicated that XopQ might interact with XopG via its 14-3-3 binding motif, encompassing the T222 residue. Indeed, interaction studies confirmed that XopQ T222 was important for interaction not only with XopG, but also with XopV, XopP, and XopX. The observation that all four proteins (XopG, XopP, XopV, and XopX) interacted at XopQ T222 suggests the possibility that competitive binding may be taking place at this residue. Furthermore, the XopQ T222A mutant, which was defective in interaction with XopX, was also defective in induction of immune responses when coexpressed with XopX.

Docking studies indicated that the XopG E76 residue might be involved in the interaction with XopQ. Interaction studies indicated that both XopG E76 and the conserved E85 residue in the conserved motif HEXXH are important for interaction with both XopQ and XopX as well as for suppression of XopQ–XopX-induced immune responses. XopG is required for virulence of *X. oryzae* pv. *oryzae* and the XopG E76 and XopG E85 residues appear to be important for this virulence-promoting activity. Taken together, our observations point towards a complex network of regulation that controls the expression, localization, and activity of these effectors in disease progression and sheds light on the role of XopG in suppression of ETI. Further studies are required to gain better insights into how *X. oryzae* pv. *oryzae* regulates these processes to cause disease.

4 | EXPERIMENTAL PROCEDURES

4.1 | Bacterial strains and plant material

The bacterial strains *E. coli* DH5α, *A. tumefaciens* AGL1, and *X. oryzae* pv. *oryzae* BXO43 (Thieme et al., 2005) were used for this study. *E. coli* and *A. tumefaciens* strains were grown in Luria Bertani (LB) medium at 37°C and 28°C, respectively. *X. oryzae* pv. *oryzae* strains were grown on peptone sucrose (PS) medium at 28°C (Ray et al., 2000). *Saccharomyces cerevisiae* PJ694a (James et al., 1996) was grown at 30°C in yeast extract, peptone, dextrose (YPD) medium or minimal media supplemented with suitable amino acids for auxotrophic selection. The plant cultivars used were the rice variety Taichung Native 1 (TN1; susceptible to *X. oryzae* pv. *oryzae* infection) for transient overexpression studies in rice and *Nicotiana benthamiana* for ectopic expression of proteins for the BiFC assay. Rice plants were kept in a greenhouse in the following conditions: approximately 30°C/25°C (day/night), approximately 80% humidity, and natural sunlight. The concentrations of antibiotics used were rifampicin (Rif) 50 μg/ml, spectinomycin (Sp) 50 μg/ml, gentamycin (Gent) 10 μg/ml, ampicillin (Amp) 100 μg/ml, and kanamycin (Km) 15 μg/ml for *X. oryzae* pv. *oryzae* and 50 μg/ml for *E. coli*.

4.2 | Vector construction and site-directed mutagenesis

Site-directed mutagenesis was done in *xopG* based on docking studies performed. The E76 and E85 residues of *xopG* were mutagenized to alanine using primers as listed in Table S1. The pENTR::*xopG* plasmid was used as template. Further cloning in yeast two-hybrid vector or BiFC-compatible vector was done using Gateway cloning (Invitrogen). Plasmids were purified using the alkaline lysis method. Gel extractions were carried out using Macherey Nagel Gel Extraction kits. Agarose gel electrophoresis, transformation of *E. coli*, and electroporation of plasmids into *A. tumefaciens* AGL1 were performed as described previously (Ray et al., 2000). All clones (Table S2) were confirmed by sequencing (ABI Prism 3700 automated DNA sequencer). The obtained sequences were subjected to homology searches using the BLAST algorithm in the National Centre for Biotechnology Information database (Altschul et al., 1990).

The *xopG* gene of *X. oryzae* pv. *oryzae* was disrupted by homologous plasmid integration using the vector pK18mob (Schäfer et al., 1994). A 310-bp fragment from the coding region of the *xopG* gene was amplified by PCR (primers xopG pk18mob EcoRI F and xopG pk18mob HindIII R; Table S1) and cloned into the *Eco*RI and *Hin*dIII sites of pK18mob. The resultant clone (pk18mob::*xopG*; Table S2) was transferred into *X. oryzae* pv. *oryzae* BXO43 by electroporation, and integration of the plasmid was selected by growth on PS medium containing rifampicin and kanamycin. Gene disruption was confirmed by PCR using a combination of gene-specific primers (xopG F and xopG R; Table S1) and vector-specific primers (M13F and M13R; Table S1). One mutant clone (*xopG*$^-$) was chosen for further study. To complement *xopG*$^-$, the wild-type *xopG* gene, *xopG E76A*, or *xopG E85A* were cloned into the *Hin*dIII and*Kpn*I sites of the pHM1 vector (Innes et al., 1988) using gene-specific primers (xopG pHM1 HindIII F and xopG pHM1 KpnI R; Table S1), yielding pHM1::*xopG*, pHM1::*xopG E76A* and pHM1::*xopG E85A* (Table S2). The pHM1 vector or the resultant clones were individually introduced into the *xopG*$^-$ strain by electroporation.

4.3 | Expression analysis of *X. oryzae* pv. *oryzae* effectors in planta

TN1 rice plants (60 days old) were clip-inoculated with *X. oryzae* pv. *oryzae* BXO43 at OD_{600} = 1. Leaf samples of 2 cm length were

collected from the site of clipping at 2, 6, 10, and 14 dpi. Leaves from the lesion zone and the leading edge of the lesion were separately collected at 10 and 14 dpi. Total RNA from the leaf samples was isolated using the NucleoSpin RNA extraction kit (Machery-Nagel). One microgram of total RNA was used for first-strand cDNA synthesis using the PrimeScript first-strand cDNA Synthesis Kit (Takara Bio) with random hexamer primers. Quantitative PCR was performed using Power SYBR Green Master Mix (Thermo Fisher Scientific) in a CFX384 RT-PCR instrument (Bio-Rad Laboratories). The gene expression values were normalized with respect to 16S rRNA and the relative expression values of the genes were calculated using the $2^{-\Delta Ct}$ method.

4.4 | Bioinformatic analysis of XopG

Multiple sequence alignment of XopG from various bacterial strains was carried out using Clustal Omega (Madeira et al., 2019) and visualized using ESPript software (Robert & Gouet, 2014). The GenBank ID of the XopG homolog in *Xanthomonas campestris* pv. *vesicatoria* 85-10 is CAJ22929.1, that of *Acidovorax citrulli* AAC00-1 is ABM33444.1, that of *P. syringae* pv. *syringae* B728a is AAY36933.1, that of *P. syringae* pv. *tomato* T1 is EEB56600.1, that of *Ralstonia solanacearum* GMI1000 is CAD17078.1, and that of *R. solanacearum* MolK2 is CAQ37632.1. The NCBI reference sequence for the XopG homolog from *Brenneria rubrifaciens* is WP_137712733.1, that of *Pantoea* sp. 201603H is WP_195761682.1, and that of *Cedecea neteri* is WP_052050207.1. For modelling of XopG, SWISS-MODEL was used in the automated mode (Waterhouse et al., 2018). For docking of the XopG model and the XopQ crystal structure, the ZDOCK online tool was used (Pierce et al., 2014). Subcellular localization prediction was carried out using NLS Mapper software (Kosugi et al., 2009).

4.5 | Codon usage pattern

The codon usage pattern was calculated for each gene to estimate the frequency of codon usage for different amino acids as described previously (Patil & Sonti, 2004), with modifications. Briefly, eight amino acids (glycine, valine, threonine, leucine, arginine, serine, proline, and alanine) were selected, which have at least four synonymous codons, and the percentage of codons that end with G or C was calculated for each amino acid and gene. The first group was chosen to include housekeeping genes of *X. oryzae* pv. *oryzae*. These genes encode BXO1_013815 (TonB-dependent siderophore receptor), BXO1_013910 (Xanthomonas adhesin-like protein), BXO1_006505 (diffusible signal factor synthase RpfF), BXO1_016165 (shikimate dehydrogenase), and BXO1_019245 (secreted xylanase). The LPS cluster, which was earlier shown to have come in *X. oryzae* pv. *oryzae* by horizontal gene transfer (Patil & Sonti, 2004), was used as a control group. This group consisted of five genes of the LPS cluster: BXO1_014260 (*smtA*), BXO1_014255 (*wxoA*), BXO1_014250 (*wxoB*), BXO1_014240 (*wxoC*), and BXO1_014235 (*wxoD*).

4.6 | Yeast two-hybrid assays

Wild-type *xopQ*, *xopQ T222A*, or *xopX* cloned in the yeast two-hybrid vector pDEST32 (Invitrogen) was used from a previous study (Deb et al., 2019, 2020). *xopU*, *xopV*, *xopP*, *xopG*, *xopG E76A*, *xopG E85A*, and *avrBs2* were cloned in the yeast two-hybrid vector pDEST22 (Invitrogen) by Gateway cloning (Invitrogen). These plasmids were transformed into *S. cerevisiae* PJ694a. Yeast transformation was done using the LiAc/single-strand carrier DNA/polyethylene glycol method (Gietz & Schiestl, 2007) with changes as described previously (Deb et al., 2019). Each set was repeated three times.

4.7 | BiFC

The wild-type copy of *xopQ*, *xopQ T222A*, or *xopX* cloned in the BiFC vector pDEST-VYNE(R)GW carrying nVFP (Gehl et al., 2009) was used from a previous study (Deb et al., 2019, 2020). *xopU*, *xopV*, *xopP*, *xopG*, *xopG E76A*, *xopG E85A*, and *avrBs2* were cloned in the BiFC vector pDEST-VYCE(R)GW (Gehl et al., 2009) carrying the C-terminal region of VFP (cVFP) by Gateway cloning (Invitrogen) to yield the constructs as listed in Table S2. These binary vectors obtained were then electroporated into *A. tumefaciens* AGL1. A suspension of two strains expressing the gene-nVFP/cVFP fusions were used for BiFC experiments as described earlier, in onion epidermal peels or in *N. benthamiana* (Deb et al., 2020). VFP signals were examined 48 h after infiltration under an LSM880 confocal microscope (Carl Zeiss) using 20× objectives and a He-Ne laser at 488 nm excitation for *Nicotiana* leaves and using 10× objectives and a GFP filter (Nikon) for onion epidermal peels. Confocal images were analysed using ZEN software. Each set was repeated three times.

4.8 | In vivo pulldown assay

Ni^{2+}-NTA-based affinity pulldown assays were performed as described previously (Deb et al., 2020). Briefly, *xopU*, *xopV*, and *xopG* were cloned with the EGFP tag in the pH7WGF2 vector. EGFP::*gus* was used from a previous study as a control (Deb et al., 2020). *xopX* was cloned with a 6×His tag in the pMDC7 vector (Table S2). pMDC7::*xopQ*-6×His was used from a previous study (Deb et al., 2020). Roots of 4-day-old TN-1 rice seedlings were cocultured with the respective bacterial suspensions of AGL1. Total protein was isolated, and in vivo pulldown was carried out using Ni^{2+}-NTA beads 24 h after cocultivation. Western blot analysis was performed using alkaline phosphatase-conjugated anti-His antibody (Sigma Aldrich) and anti-GFP antibody (Abcam). For immunoblotting, alkaline phosphatase conjugated to anti-rabbit immunoglobulin G secondary antibody (Sigma Aldrich), 4-nitroblue tetrazolium (NBT; Roche), and 5-bromo-4-chloro-3-indolyl-phosphate 4-toluidine salt (BCIP; Roche) were used.

4.9 | Callose deposition in rice

Callose deposition assays were done as described earlier (Deb et al., 2019; Sinha et al., 2013). Callose was imaged in an epifluorescence microscope (Nikon) using a blue filter (excitation wavelength of 365 nm) and a 10× objective. The number of callose deposits per leaf was counted, excluding the zone of infiltration. Statistical analysis for significance was conducted using the unpaired two-sided Student's *t* test. At least five leaves were imaged for each construct per experiment. Each set was repeated three times.

4.10 | Defence response-associated PCD assay

Assays for PCD in rice roots were performed as described earlier (Deb et al., 2019; Sinha et al., 2013). The samples were visualized under an LSM880 confocal microscope (Carl Zeiss) using 63× oil immersion objectives and a He-Ne laser at 543 nm excitation to detect PI internalization. Images were analysed using ZEN software. At least five roots were imaged for each construct per experiment. Each set was repeated three times. Quantification of PI internalization was carried out using ImageJ software (Schneider et al., 2012). For quantification, a region of interest was defined internal to the cell wall, and cell fluorescence was calculated, factoring in the integrated density of fluorescence, area of region of interest, and background fluorescence.

4.11 | Virulence assay

Susceptible TN1 rice plants (60 days old) were used for assays for virulence. *X. oryzae* pv. *oryzae* strains were grown to saturation and inoculated by dipping scissors into bacterial cultures of OD_{600} = 1 and clipping the tips of rice leaves. Lesion lengths were measured at 14 dpi and expressed as the mean lesion length with standard deviation.

4.12 | Western blotting for XopG expression

Roots of 4-day-old TN1 rice plants were cocultured with bacterial suspension of *A. tumefaciens* AGL1 alone or AGL1 harbouring the constructs expressing the XopG wild-type protein or its mutants, XopG E76A or XopG E85A. Sixteen hours after coculture, total protein was isolated in lysis buffer as described earlier (Gupta et al., 2015). Equal amounts of total protein supernatants were used for western blot analysis using anti-GFP antibody (1:2000 dilution; Abcam). Immunoblotting for EGFP-tagged protein was carried out using alkaline phosphatase-conjugated anti-rabbit immunoglobulin G secondary antibody (Sigma Aldrich). Equal loading of protein in the different samples was shown using Coomassie blue staining of gels.

ACKNOWLEDGEMENTS

This work was supported by grants to H.K.P. from the Council of Scientific and Industrial Research (CSIR), Government of India (MLP0121). R.V.S. was supported by the J. C. Bose Fellowship from the Science and Engineering Research Board (SERB), Government of India (GAP0444).

CONFLICT OF INTEREST

The authors declare that no conflict of interest exists.

AUTHOR CONTRIBUTIONS

S.D., H.K.P., and R.V.S. conceived and designed the experiments. S.D. performed the biological assays and wrote the manuscript. R.N. performed the structural docking studies. C.G.G. performed the in planta gene expression analysis. S.D., H.K.P., and R.V.S. analysed the data and finalized the manuscript, which was approved by all the authors. H.K.P. and R.V.S. contributed reagents/materials.

DATA AVAILABILITY STATEMENT

All data have been included in the manuscript.

ORCID

C. G. Gokulan https://orcid.org/0000-0002-4305-2818
Ramesh V. Sonti https://orcid.org/0000-0003-4845-0601

REFERENCES

Altschul, S.F., Gish, W., Miller, W., Myers, E.W. & Lipman, D.J. (1990) Basic local alignment search tool. *Journal of Molecular Biology*, 215, 403–410.

Baruch, K., Gur-Arie, L., Nadler, C., Koby, S., Yerushalmi, G., Ben-Neriah, Y. et al. (2011) Metalloprotease type III effectors that specifically cleave JNK and NF-κB. *EMBO Journal*, 30, 221–231.

Block, A., Toruño, T.Y., Elowsky, C.G., Zhang, C., Steinbrenner, J., Beynon, J. et al. (2014) The *Pseudomonas syringae* type III effector HopD1 suppresses effector-triggered immunity, localizes to the endoplasmic reticulum, and targets the *Arabidopsis* transcription factor NTL9. *New Phytologist*, 201, 1358–1370.

Deb, S., Ghosh, P., Patel, H.K. & Sonti, R.V. (2020) Interaction of the *Xanthomonas* effectors XopQ and XopX results in induction of rice immune responses. *The Plant Journal*, 104, 332–350.

Deb, S., Gupta, M.K., Patel, H.K. & Sonti, R.V. (2019) *Xanthomonas oryzae* pv. *oryzae* XopQ protein suppresses rice immune responses through interaction with two 14-3-3 proteins but its phospho-null mutant induces rice immune responses and interacts with another 14-3-3 protein. *Molecular Plant Pathology*, 20, 976–989.

Deb, S., Kumar, C., Kumar, R., Kaur, A., Ghosh, P. & Jha, G. et al. (2021) A bacterial derived plant- mimicking cytokinin hormone regulates social behaviour in a rice pathogen. *bioRxiv*, doi: 10.1101/2021.07.05.451090 [preprint].

Gehl, C., Waadt, R., Kudla, J., Mendel, R.R. & Hansch, R. (2009) New GATEWAY vectors for high throughput analyses of protein–protein interactions by bimolecular fluorescence complementation. *Molecular Plant*, 2, 1051–1058.

Gietz, R.D. & Schiestl, R.H. (2007) High-efficiency yeast transformation using the LiAc/SS carrier DNA/PEG method. *Nature Protocols*, 2, 31–34.

Gupta, M.K., Nathawat, R., Sinha, D., Haque, A.S., Sankaranarayanan, R. & Sonti, R.V. (2015) Mutations in the predicted active site of *Xanthomonas oryzae* pv. *oryzae* XopQ differentially affect virulence,

suppression of host innate immunity, and induction of the HR in a nonhost plant. *Molecular Plant-Microbe Interactions*, 28, 195–206.
Hajri, A., Brin, C., Hunault, G., Lardeux, F., Lemaire, C., Manceau, C., et al. (2009) A "repertoire for repertoire" hypothesis: repertoires of type three effectors are candidate determinants of host specificity in *Xanthomonas*. *PLoS One*, 4, e6632.
Hauck, P., Thilmony, R. & He, S.Y. (2003) A *Pseudomonas syringae* type III effector suppresses cell wall-based extracellular defense in susceptible *Arabidopsis* plants. *Proceedings of the National Academy of Sciences of the United States of America*, 100, 8577–8582.
Innes, R.W., Hirose, M.A. & Kuempel, P.L. (1988) Induction of nitrogen-fixing nodules on clover requires only 32 kilobase pairs of DNA from the *Rhizobium trifolii* symbiosis plasmid. *Journal of Bacteriology*, 170, 3793–3802.
James, P., Halladay, J. & Craig, E.A. (1996) Genomic libraries and a host strain designed for highly efficient two-hybrid selection in yeast. *Genetics*, 144, 1425–1436.
Jones, J.D. & Dangl, J.L. (2006) The plant immune system. *Nature*, 444, 323–329.
Kaur, A., Bansal, K., Kumar, S., Sonti, R.V. & Patil, P.B. (2019) Complete genome dynamics of a dominant-lineage strain of *Xanthomonas oryzae* pv. *oryzae* harbouring a novel plasmid encoding a type IV secretion system. *Access Microbiology*, 1, e000063.
Kim, J.F., Charkowski, A.O., Alfano, J.R., Collmer, A. & Beer, S.V. (1998) Sequences related to transposable elements and bacteriophages flank avirulence genes of *Pseudomonas syringae*. *Molecular Plant-Microbe Interactions*, 11, 1247–1252.
Kosugi, S., Hasebe, M., Tomita, M. & Yanagawa, H. (2009) Systematic identification of cell cycle-dependent yeast nucleocytoplasmic shuttling proteins by prediction of composite motifs. *Proceedings of the National Academy of Sciences of the United States of America*, 106, 10171–10176.
Liu, Y., Long, J., Shen, D. & Song, C. (2016) *Xanthomonas oryzae* pv. *oryzae* requires H-NS-family protein XrvC to regulate virulence during rice infection. *FEMS Microbiology Letters*, 363, fnm067.
Ma, W., Dong, F.F.T., Stavrinides, J. & Guttman, D.S. (2006) Type III effector diversification via both pathoadaptation and horizontal transfer in response to a coevolutionary arms race. *PLoS Genetics*, 2, e209.
Madeira, F., Park, Y.M., Lee, J., Buso, N., Gur, T., Madhusoodanan, N. et al. (2019) The EMBL-EBI search and sequence analysis tools APIs in 2019. *Nucleic Acids Research*, 47, W636–W641.
Midha, S., Bansal, K., Kumar, S., Girija, A.M., Mishra, D., Brahma, K. et al. (2017) Population genomic insights into variation and evolution of *Xanthomonas oryzae* pv. *oryzae*. *Scientific Reports*, 7, 40694.
Patil, P.B. & Sonti, R.V. (2004) Variation suggestive of horizontal gene transfer at a lipopolysaccharide (*lps*) biosynthetic locus in *Xanthomonas oryzae* pv. *oryzae*, the bacterial leaf blight pathogen of rice. *BMC Microbiology*, 4, 40.
Pierce, B.G., Wiehe, K., Hwang, H., Kim, B.H., Vreven, T. & Weng, Z. (2014) ZDOCK server: interactive docking prediction of protein–protein complexes and symmetric multimers. *Bioinformatics*, 30, 1771–1773.
Ray, S.K., Rajeshwari, R. & Sonti, R.V. (2000) Mutants of *Xanthomonas oryzae* pv. *oryzae* deficient in general secretory pathway are virulence deficient and unable to secrete xylanase. *Molecular Plant-Microbe Interactions*, 13, 394–401.
Robert, X. & Gouet, P. (2014) Deciphering key features in protein structures with the new ENDscript server. *Nucleic Acids Research*, 42, W320–W324.
Rohmer, L., Guttman, D.S. & Dangl, J.L. (2004) Diverse evolutionary mechanisms shape the Type III effector virulence factor repertoire in the plant pathogen *Pseudomonas syringae*. *Genetics*, 167, 1341–1360.
Rufián, J.S., Lucía, A., Rueda-Blanco, J., Zumaquero, A., Guevara, C.M., Ortiz-Martín, I. et al. (2018) Suppression of HopZ effector-triggered plant immunity in a natural pathosystem. *Frontiers in Plant Science*, 9, 977.
Schäfer, A., Tauch, A., Jäger, W., Kalinowski, J., Thierbach, G. & Pühler, A. (1994) Small mobilizable multi-purpose cloning vectors derived from the *Escherichia coli* plasmids pK18 and pK19: selection of defined deletions in the chromosome of *Corynebacterium glutamicum*. *Gene*, 145, 69.–73.
Schneider, C.A., Rasband, W.S. & Eliceiri, K.W. (2012) NIH Image to ImageJ: 25 years of image analysis. *Nature Methods*, 9, 671–675.
Sinha, D., Gupta, M.K., Patel, H.K., Ranjan, A. & Sonti, R.V. (2013) Cell wall degrading enzyme induced rice innate immune responses are suppressed by the type 3 secretion system effectors XopN, XopQ, XopX and XopZ of *Xanthomonas oryzae* pv. *oryzae*. *PLoS One*, 8, e75867.
Thieme, F., Koebnik, R., Bekel, T., Berger, C., Boch, J., Buttner, D. et al. (2005) Insights into genome plasticity and pathogenicity of the plant pathogenic bacterium *Xanthomonas campestris* pv. *vesicatoria* revealed by the complete genome sequence. *Journal of Bacteriology*, 187, 7254–7266.
Waterhouse, A., Bertoni, M., Bienert, S., Studer, G., Tauriello, G., Gumienny, R. et al. (2018) SWISS-MODEL: homology modelling of protein structures and complexes. *Nucleic Acids Research*, 46, W296–W303.
Wei, C.-F., Kvitko, B.H., Shimizu, R., Crabill, E., Alfano, J.R., Lin, N.-C. et al. (2007) A *Pseudomonas syringae* pv. *tomato* DC3000 mutant lacking the type III effector HopQ1-1 is able to cause disease in the model plant *Nicotiana benthamiana*. *The Plant Journal*, 51, 32–46.

SUPPORTING INFORMATION

Additional supporting information may be found in the online version of the article at the publisher's website.

How to cite this article: Deb, S., Gokulan, C.G., Nathawat, R., Patel, H.K. & Sonti, R.V. (2022) Suppression of XopQ–XopX-induced immune responses of rice by the type III effector XopG. *Molecular Plant Pathology*, 23, 634–648. https://doi.org/10.1111/mpp.13184